Power Flow Analysis of Advanced Power Generation Centre for More Electric Aircraft

Ge Bai
Power Electronics and Machines Centre (PEMC) Research Group
Faculty of Engineering
University of Nottingham
Nottingham, UK
ge.bai@nottingham.ac.uk

Tao Yang
Power Electronics and Machines Centre (PEMC) Research Group
Faculty of Engineering
University of Nottingham
Nottingham, UK
tao.yang@nottingham.ac.uk

Seang Shen Yeoh
Power Electronics and Machines Centre (PEMC) Research Group
Faculty of Engineering
University of Nottingham
Nottingham, UK
seang.yeoh@nottingham.ac.uk

Serhiy Bozhko
Power Electronics and Machines Centre (PEMC) Research Group
Faculty of Engineering
University of Nottingham
Nottingham, UK
serhiy.bozhko@nottingham.ac.uk

Patrick Wheeler
Power Electronics and Machines Centre (PEMC) Research Group
Faculty of Engineering
University of Nottingham
Nottingham, UK
pat.wheeler@nottingham.ac.uk

***Abstract*—The more-electric aircraft (MEA) has been seen as the most major trend in the aerospace industry. With the increase in electrified loads, there is the need to generate more electrical power on-board aircraft. Considering regional jet sized aircraft, one novel approach is to extract electric power from high-pressure shaft as well as the low-pressure shaft within a multi-spool aircraft engine. This allows for more electrical power extraction within the engine shaft mechanical limits. Furthermore, it opens opportunities to enable power transfer between two different shafts within the engine in order to increase the operational margin and improve efficiency. This system called the Advanced Power Generation Centre (APGC), is introduced in this paper and the associated electrical subsystem with the high-pressure shaft has been analysed in detail. The capabilities and limitations of this topology have been discussed in this paper and validated in MATLAB/Simulink environment.**

Keywords—More Electronic Aircraft, Advanced Power Generation Centre, back-to-back converter.

I. INTRODUCTION

The main idea of More-Electric Aircraft (MEA) to realise aircraft electrification is by relying more on electrical power to gradually replace the three other types of power: pneumatic, hydraulic, and mechanical. The idea of using electrical power to replace other types of power was initially proposed by NASA and the U.S Air Force in the program of Advanced Short-Haul Transport (ASHT)[1]. This program explored the potential technologies of using electrical systems to replace traditional hydraulic and pneumatic systems to achieve the target of improving the overall efficiency, performance, and reliability in the short-haul transport aircraft in the early 1970s. Since then, with the significant improvements in the area of power electronics, aerodynamics, and thermal management, the MEA has continued to evolve with benefits in high efficiency, reliability and design flexibility, low maintenance cost, and reduced emissions [2]. At present time, it is a good opportunity to rebuild a greener and more efficient air transport to meet the net zero flying 2050 climate change challenge [3-5].

To meet the increasing electrical power demand on the aircraft, the advanced power generation centre (APGC) is proposed in this paper [6, 7]. It consists of power electronic drive systems interfaced between the multi-spool aircraft engine and the primary electrical distribution bus as seen in Fig. 1. Generally, this topology can be divided into two channels: high-pressure (HP) channel and low-pressure (LP) channel. Each channel includes a generator, a corresponding main DC bus connected converter and a part of a back-to-back (B2B) converter. This topology enables not only power to be extracted from both channels to feed the main bus, but also increasing the aircraft engine compressor' surge margin [6]. The B2B converter allows power to be transferred between the channels.

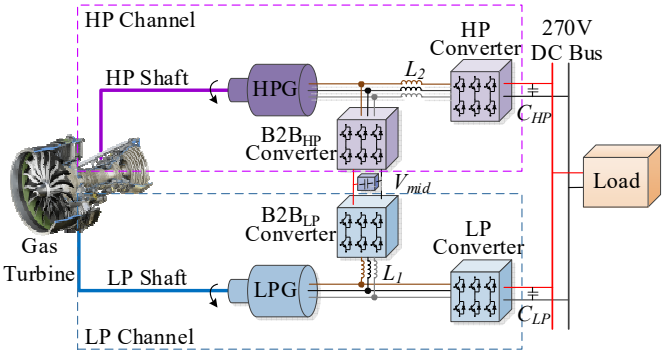

Fig. 1. The proposed APGC for MEA applications.

Based on whether there is power flow through the B2B converter, there are two operation modes: coordinated power offtake (CPO) mode and electric power transfer (EPT) mode. These two operation modes not only improve the system's fault tolerance ability but also improve the efficiency of fossil fuel's utilization. Additionally, the $B2B_{HP}$ converter could be used to control the operation of the high-pressure shaft generator (HPG) without field weakening operation due to higher DC side terminal voltage, hence there is no need to inject reactive current to the HPG.

Initial findings have shown that the amount of power transferred to HP converter may have a potential limitation from the power flow aspect due to the inductance element of the generator system and the high operating speed. This may result in system instability as the power demand may exceed

the generator capabilities. Hence, the potential power flow limitation of the APGC is under research in this paper.

The paper is organized as follows: in Section II the HPG and HP converter are analysed in order to determine their power flow limitation. In section III, the control strategies for both channels are introduced, followed by further analysis of power limitation. Validations at different operating situations are done in section IV as simulation results. Finally, the conclusions of the whole paper are summarized in Section V.

II. Power Flow Between High-Pressure Generator and High-Pressure Converter

Before going through the full APGC topology, a simple analysis needs to be performed to proof the power transfer limitation can exist. The power flow between HPG and HP converter and its topology is used for study within this Section as shown in Fig.2.

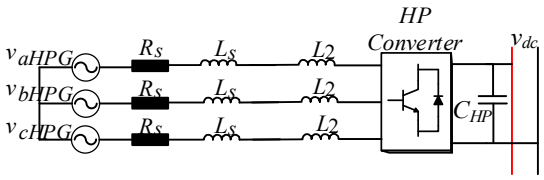

Fig. 2. The equivalent circuit of HPG and HP converter.

The HP converter is a two-level converter where SVPWM modulation method is applied. To avoid converter over modulation, the $|V|_{\max}$ of converter needs to meet the limitation listed below [8, 9]:

$$|V|_{\max} \le \frac{v_{dc}}{\sqrt{3}} \tag{1}$$

where $|V|_{\max}$ is the maximum value of the fundamental phase voltage of the converter; v_{dc} is the main DC bus voltage.

Then, Fig.2 can therefore be simplified as it is shown in Fig.3.

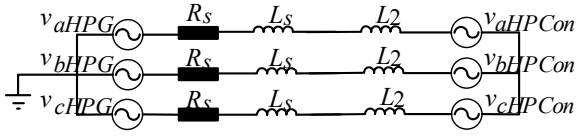

Fig. 3. The improved equivalent circuit of HPG and HP converter.

where R_s is the stator resistance; L_s is the stator inductance; L_2 is the inductance of the inductor deployed at the front end of the HP converter.

The following equations related to the Fig.3 is listed below.

$$v_{aHPG} = \omega_{eHP}\psi_m \cos(\omega_{eHP}t) \tag{2}$$

$$v_{bHPG} = \omega_{eHP}\psi_m \cos(\omega_{eHP}t - \frac{2pi}{3}) \tag{3}$$

$$v_{cHPG} = \omega_{eHP}\psi_m \cos(\omega_{eHP}t + \frac{2pi}{3}) \tag{4}$$

where ω_{eHP} is the electrical angular speed of HPG; ψ_m is the rotor flux linkage of permanent magnet.

To simplify calculation process, the equivalent circuit of phase *a* is demonstrated in Fig. 4.

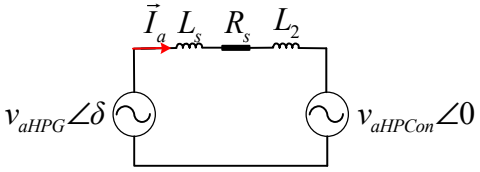

Fig. 4. The equivalent circuit of phase *a*, only has HPG and HP converter.

where v_{aHPG} and v_{aHPCon} are the magnitudes of the two voltage sources, and $\vec{v}_{aHPG}$ leads $\vec{v}_{aHPCon}$ by angle δ. The impedance is:

$$\vec{Z} = R_s + j\omega_{eHP}(L_s + L_2) = Z\angle\theta \tag{5}$$

where *j* represents the imaginary number. As it is shown by the impedance triangle wherein,

$$\theta = \tan^{-1}\frac{\omega_{eHP}(L_s + L_2)}{R_s} \tag{6}$$

The armature current in Fig.4 can be expressed as:

$$\vec{I}_a = \frac{v_{aHPG}\angle\delta - v_{aHPCon}\angle 0}{Z\angle\theta} \tag{7}$$

The complex power received by the HP converter can be calculated by[8]:

$$\vec{S}_{HPCon} = \frac{1}{2}\vec{v}_{aHPCon}\vec{I}^* = P_{HPCon} + jQ_{HPCon} \tag{8}$$

$$P_{HPCon} = -\frac{v_{aHPCon}^2}{2Z}R_s + \frac{v_{aHPG}v_{aHPCon}}{2Z}\sin(\delta + \frac{\pi}{2} - \theta) \tag{9}$$

$$Q_{HPCon} = -\frac{v_{aHPCon}^2}{2Z}(L_s + L_2) + \frac{v_{aHPG}v_{aHPCon}}{2Z}\cos(\delta + \frac{\pi}{2} - \theta) \tag{10}$$

where *j* is the complex operator; *S* is the apparent power which provides active (*P*) and reactive power (*Q*); $\vec{I}^*$ is the conjugate complex numbers of $\vec{I}$. For sine wave signal, the root mean square (RMS) value is $1/\sqrt{2}$ of its magnitude value. Both voltage and current signals applied are sine wave signals, hence, there is a coefficient in (8).

In (9), the value of R_s is quite small comparing to the value of *Z*. Equation (9) can be updated to:

$$P_{HPCon-update} = \frac{v_{aHPG}v_{aHPCon}}{2Z}\sin(\delta) \tag{11}$$

It can be observed from (9), the maximum power transferred to HP converter is $\frac{v_{aHPG}v_{aHPCon}}{2Z}$, under the condition that $\vec{v}_{aHPG}$ is 90 degree ahead to $\vec{v}_{aHPCon}$.

III. Power Flow Limitation in Both Channels

A. Power Flow Limitation in HP Channel

The topology of HP channel is shown in Fig.5. In HP channel, the HPG, $B2B_{HP}$ converter and HP converter are

included. The series inductors are placed in the end front of HP converter. Since the $B2B_{HP}$ converter is directly connected with HPG and the DC voltage value within the B2B converter can be set to a very high value, which leads to no flux weakening requirement for the HPG. Constant power loads are employed to the HVDC bus to represent the aircraft loads. The HP converter is used to control the amount of power used to feed the load and to maintain the main DC bus voltage.

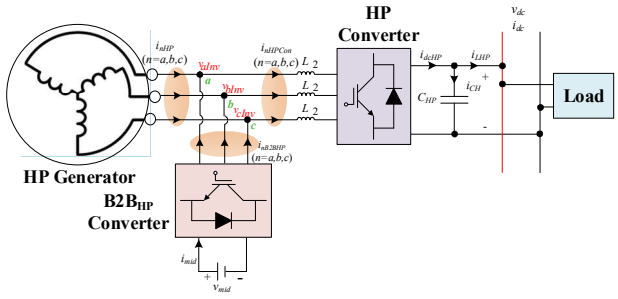

Fig. 5. High-pressure channel topology.

Assuming that the HPG is a three phase permanent magnet synchronous generator (PMSG), the voltage equations in *dq* frame are as follows[10]:

$$v_{dHP} = -R_s i_{dHP} - L_d \frac{d}{dt} i_{dHP} + L_q \omega_{eHP} i_{qHP} \tag{12}$$

$$v_{qHP} = -R_s i_{qHP} - L_q \frac{d}{dt} i_{qHP} + (-L_d i_{dHP} + \psi_m)\omega_{eHP} \tag{13}$$

where v_{dHP} and v_{qHP} are stator voltages in *dq* axes respectively; i_d and i_q are *dq* axes stator currents; L_d and L_q are *dq* axes stator inductances. For a surface mounted PMM, L_d=L_q=L_s.

As can be observed from Fig.5, there are three current branches: HPG side branch, HP converter side branch, and B2B converter side branch. These three branches share the same junction points and connected in parallel. Based on Kirchhoff's voltage law (KVL), in the HP converter side branch, the voltage of electronic components have the following relationship:

$$\vec{v}_{inv} = \vec{v}_{L2} + \vec{v}_{HPCon} \tag{14}$$

where $\vec{v}_{inv}$ is the phasor voltage of the junction points, $\vec{v}_{L2}$ is the phasor voltage over the inductor L_2, and $\vec{v}_{HPCon}$ is the phasor voltage of the AC terminal of HP converter. The detailed information of each component are described as follows:

$$\vec{v}_{inv} = \vec{v}_{dHP} + \vec{v}_{qHP} \tag{15}$$

$$\vec{v}_{L2} = \omega_{eHP} L_2 \vec{i}_{HPCon} \tag{16}$$

Based on the Kirchhoff's current law (KCL), the relationship among the three branches currents is listed below:

$$\vec{i}_{HP} = \vec{i}_{B2BHP} + \vec{i}_{HPCon} \tag{17}$$

Since there is no flux weakening control for HPG, i_d=0, thus:

$$\vec{i}_{HP} = \vec{i}_{qHP} \tag{18}$$

Assuming steady state operation and ignoring R_s, (12) and (13) can be simplified to:

$$v_{dHP} = L_q \omega_{eHP} i_{qHP} \tag{19}$$

$$v_{qHP} = \psi_m \omega_{eHP} \tag{20}$$

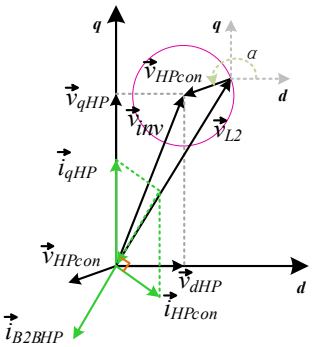

Fig. 6. Voltage phasor diagram of HP Converter branch and currents phasors among three branches.

Based on (14) ~ (20), the voltage phasors diagram of HP converter branch and current phasors among the three branches are drawn in Fig.6. The green lines represent the phasors of three branches currents in (17), and the black lines are the phasors of voltages in (14), the pink circle is the locus of terminal voltage phasor over the inductance; α represents the rotating angle of $\vec{v}_{HPCon}$.

1) Voltage Phasors Identification

Based on the PMSG dynamic equations (12) and (13), the $\vec{v}_{inv}$ can be easily identified, where it is the sum vector voltage of v_{dHP} and v_{qHP}.

$$\vec{v}_{inv} = \omega_{eHP} L_q i_{qHP} + j\omega_{eHP}\psi_m \tag{21}$$

Due to high-speed operation of HPG and hence high resulting back-EMF, proper control method has been applied to HP converter to maintain magnitude of AC side voltage of HP converter to meet requirement listed in (1).

$$\vec{v}_{HPCon} = -\frac{v_{dc}}{\sqrt{3}}\cos(\alpha) - j\frac{v_{dc}}{\sqrt{3}}\sin(\alpha) \tag{22}$$

Based on (14), the voltage phasor over L_2 can be easily obtained.

$$\vec{v}_{L2} = \left(\frac{v_{dc}}{\sqrt{3}}\cos(\alpha) + \omega_{eHP} L_q i_q\right) + j\left(\frac{v_{dc}}{\sqrt{3}}\sin(\alpha) + \omega_{eHP}\psi_m\right) \tag{23}$$

Now, the three voltage phasors have been obtained, the next is to calculate the three branches current phasors.

2) Current Phasors Identification

The HPG side branch current has already shown in (18). Next is to calculate the current phasor from HP converter side branch. Since the voltage phasor of the inductor is 90 degrees ahead to its current, the current phasor of HP converter side branch can be calculated by (16):

$$\vec{i}_{HPCon} = \frac{v_{dc}\sin(\alpha)+\omega_{eHP}\psi_m}{\sqrt{3}\omega_{eHP}L_2} - j\frac{v_{dc}\cos(\alpha)+\omega_{eHP}L_q i_{qHP}}{\sqrt{3}\omega_{eHP}L_2} \quad (24)$$

Based on KCL, $\vec{i}_{B2BHP}$ can be calculated by (17), (18) and (24).

$$\vec{i}_{B2B} = -\frac{v_{dc}\sin(\alpha)+\omega_{eHP}\psi_m}{\sqrt{3}\omega_{eHP}L_2} + j\left(\frac{v_{dc}\cos(\alpha)+\omega_{eHP}L_q i_{qHP}}{\sqrt{3}\omega_{eHP}L_2} - i_{qHP}\right) \quad (25)$$

3) Three Branches Power Calculation

The three-phase complex power, S, can be written as[8]:

$$\vec{S} = \frac{3}{2}\vec{V}\vec{I}^{*} = \frac{3}{2}(P+jQ) \quad (26)$$

The voltage and current can be equated as:

$$\vec{V} = \vec{v}_d + j\vec{v}_q \quad (27)$$

$$\vec{I}^{*} = i_d - ji_q \quad (28)$$

The product of these vectors yields:

$$\vec{S} = \frac{3}{2}(v_d i_d + v_q i_q) + j\frac{3}{2}(v_q i_d - v_d i_q) \quad (29)$$

Based on (29), active power, *P*, can be calculated as:

$$P = \frac{3}{2}(v_d i_d + v_q i_q) \quad (30)$$

According to (30), the active power from three branches can be calculated. The positive current directions are signed in Fig.5. For HPG and $B2B_{HP}$ converter, when power is output through these two components, the sign signal of active power is positive. For HP converter, when the power goes through into it and feeds the main DC bus load, the active power sign signal is positive. Active power output by HPG can be calculated as:

$$P_{HPG} = \frac{3}{2}v_{qHP}i_{qHP} = \frac{3}{2}i_{qHP}\omega_{eHP}\psi_m \quad (31)$$

Active power received by HP converter can be calculated as:

$$P_{HPCon} = 1.5\vec{v}_{HPCon}\cdot\vec{i}^{*}_{HPCon} = 1.5\left(\frac{v_{dc}\sqrt{(\omega_{eHP}\psi_m)^2+(\omega_{eHP}L_q i_{qHP})^2}}{\sqrt{3}\omega_{eHP}L_2}\cos(\alpha-\lambda)\right) \quad (32)$$

where $\tan\lambda = \frac{\omega_{eHP}\psi_m}{\omega_{eHP}L_q i_{qHP}}$

It can be seen from (32), the power transferred to HP converter is mainly related two phasors, $\vec{v}_{inv}$ and $\vec{v}_{HPCon}$. If there is no power transferred from HPG to HP converter, i_{qHP} equals to 0, $\vec{v}_{inv}$ is reduced to the same with $\vec{v}_{qHP}$. In this case, (32) can be simplified to the same with (11).

Similar method can be applied to calculate the active power transferred from the B2B side branch. The calculation process is omitted, and the result is shown as follows:

$$P_{B2B} = -1.5\left(\frac{v_{dc}\sqrt{(\omega_{eHP}\psi_m)^2+(\omega_{eHP}L_q i_{qHP})^2}}{\sqrt{3}\omega_{eHP}L_2}\cos(\alpha-\lambda)\right) - 1.5i_{qHP}\omega_{eHP}\psi_m \quad (33)$$

It can be seen from (33), the power is mainly consisted by two parts, one is the power from HP converter side branch and the other is the power from HPG side branch. By adjusting the sign signal of each part, the power flow direction can be changed, correspondingly the sign signals of P_{HPG} and P_{HPCon} are changed as well.

To summarise this section, the voltage phasors and current phasors shown in Fig.6 have been all calculated. Additionally, the active power equations of the three branches are listed in (31) ~ (33). The three power's positive direction is signed in Fig.5.

B. Power Flow Limitation in LP Channel

Following the derivation process earlier in Section II, the equivalent topology of LP channel is shown in Fig.9. In LP channel, the LPG, $B2B_{LP}$ converter, and LP converter are included. The series inductors are placed in the end front of LP converter. The operation speed of LPG is under the base-speed, hence the LP converter is used to control the operation of LPG.

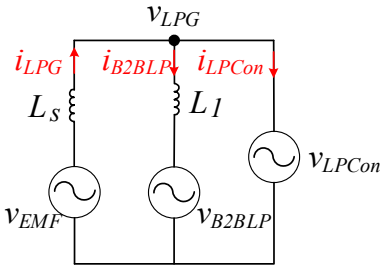

Fig. 7. The equivalent circuit of LP channel.

Based on the theory in Section II, the maximum power output by LP converter is related to the output voltage of LPG and the AC side voltage of LP converter, as it can be seen from Fig.7. There is no impedance between these two points. Hence, the power transferred to LP converter is only limited by the modulation method and the cable ampacity.

IV. Simulation Results

In this Section, the simulation verification based on the philosophies in Section II and Section III are both illustrated. Firstly, the simulation verification is based on the two simple three-phase-AC sources as illustrated in Fig.3. Then the HP channel is built in Simulink, and the verification based on (32) is achieved step by step. The process begins with the power only transferred from $B2B_{HP}$ converter to the HP converter, then both other branches transfer power to the HP converter side branch.

A. Power Transfer Limitation between Two Three-phase-AC sources

In this part, the topology of two-three-phase-AC sources is built based on Fig. 3 in MATLAB/Simulink in continuous

domain. Based on (11), when $\delta = 90^o$, where $\vec{v}_{aHPG}$ is 90 degree ahead to $\vec{v}_{aHPCon}$, $P_{HPCon\text{-}update}$ has the maximum value. The parameters based on HP channel and used to build the Simulink is listed in Table I.

TABLE I. PARAMETERS APPLIED IN FIG.3 TO VERIFIED (11)

Parameter	Symbol	Value
Electrical Angular Speed of HPG	ω_{eHP}	5.969×10^3 rad/s
Machine Flux Linkage	ψ_m	3.644×10^{-4} Wb
Main DC Bus Voltage	v_{dc}	270V
Stator Inductance	L_s	99×10^{-6} H
Stator Resistance	R_s	$1.058 \times 10^{-3}\,\Omega$
Inductance of the Inductor Deployed at the front end of HP Converter	L_2	1×10^{-4} H

Based on the parameters in Table.1 and (11), the maximum value is calculated as 42.77kW.

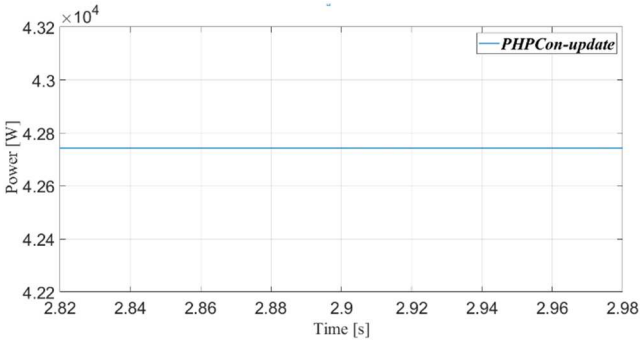

Fig. 8. Maximum power can be transferred to HPcon converter based on Fig. 3.

The system in Fig.3 is verified in time-domain. The result is shown in Fig.8, where the simulation result in the steady state is 42.74kW, which is acceptable compared to the calculation result.

B. Power Transfer Limitation among 3 three-phase-AC sources with Constant DC Bus Voltage.

In this part, the HP channel is built in MATLAB/Simulink in continuous domain, where the average model for power converters is adopted. The transmission cable impedance is omitted for the analyses.

In order to maintain consistency with sub-section *A*, the condition of the first verification is no power transferred from HPG side branch, hence the sum voltage of v_{inv} equals to the back-EMF. Additionally, the main DC bus voltage is maintained at 270V. For this purpose, a compensation term is proposed to compensate the voltage deviation caused by the droop control, and the voltage reference is given as follows:

$$v_{dc}^{*} = 270 + \frac{i_{dcHP}}{g_{HP}} \tag{34}$$

where g_{HP} is the droop gain applied in HP channel. Under this condition, (32) is simplified to,

$$P_{HPCon} = 1.5\frac{270\omega_{eHP}\psi_m}{\sqrt{3}\omega_{eHP}L_2}\cos(\alpha) \tag{35}$$

Equation (35) is compared to (11), it is worth to notice that the denominator is changed from $(L_s + L_2)$ to L_2, which means that the maximum power output by HP converter is related to its AC terminal voltage magnitude and the node position voltage and the impedance between these two voltages. Based on (35), the maximum power output by HP converter is calculated to be 85.11kW. In simulation, the load power is started from 60kW, at 0.05s it is changed to 70kW, and 0.075s it is changed to 80kW, since 0.1s the load power is increased in step increments of 1kW every 0.025s until it reaches 88kW at t = 0.2s.

TABLE II. LOAD POWER I.

Times (s)	0	0.05	0.075	0.1	0.125	0.15	0.175	0.2
Power (kW)	60	70	80	84	85	86	87	88

The result of main DC bus voltage is shown in Fig. 9.

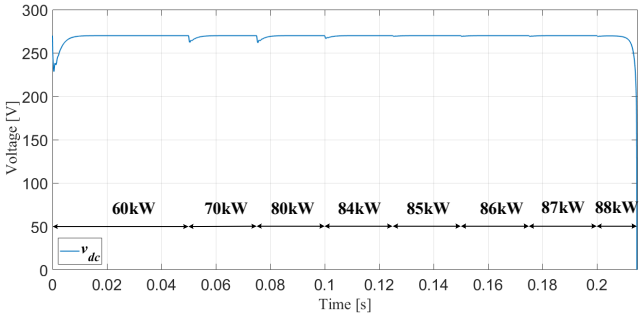

Fig. 9. Main DC bus voltage with the compensate droop control.

As it is shown in Fig. 9, the main DC bus voltage is maintained to be 270V with the load power increasing, as expected. The system reaches the unstable region when the power load increased to 88kW as it can be seen that the system is stuck at 0.215s. Compared to the calculation result, 88kW is acceptable.

C. Power Transfer Limitation among Three three-phase-AC sources with Drooped DC Bus Voltage

In this part, the system is verified under the normal droop control method, as illustrated in (36).

$$i_{dcHP}^{*} = (270 - v_{dc})g_{HP} \tag{36}$$

Under this equation, the DC bus voltage will droop with load power increasing. The maximum power transferred to the main DC bus load through the HP converter needs to meet the equation (37), where the first equation is derived from the previous theories and the second equation is derived from the droop control equation. Based on (37), the maximum power transferred to through HP converter to feed the main DC load can be calculated as 73.37kW.

$$P_{HPCon} = 1.5\frac{v_{dc}\omega_{eHP}\psi_m}{\sqrt{3}\omega_{eHP}L_2} = (270 - v_{dc})g_{HP}v_{dc} \quad (37)$$

Based on the calculation result, the load power changing with time is show in Table III. The result of main DC bus voltage is shown in Fig. 10.

TABLE III. LOAD POWER II.

Times (s)	0	0.05	0.075	0.1	0.125	0.15	0.175	0.2
Power (kW)	60	66	70	72	74	75	76	77

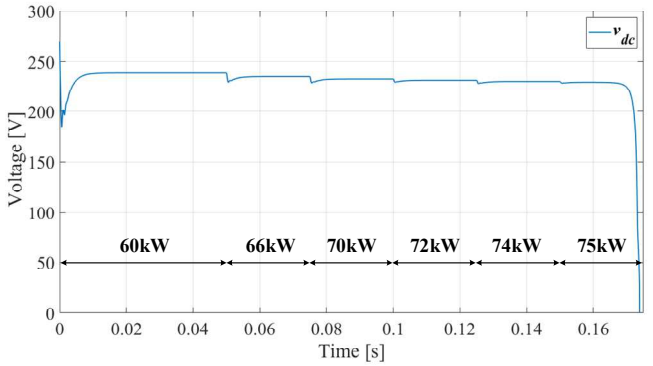

Fig. 10. Main DC bus voltage with normal droop control.

As shown in Fig.10, the Simulation is stuck at 0.174s where the load power applied is 75kW, which is approximately close to the calculated power limit.

To further verify equation (32), HPG is controlled to generate power, for example 10kW, and droop control is also applied to HP converter. Using the similar method mentioned before in this Section, the maximum power transferred to main DC bus to feed the load through HP converter can be calculated as 73.51kW. The same load power is applied to the Simulink as shown in Table III. The result of main DC bus voltage is shown in Fig. 11.

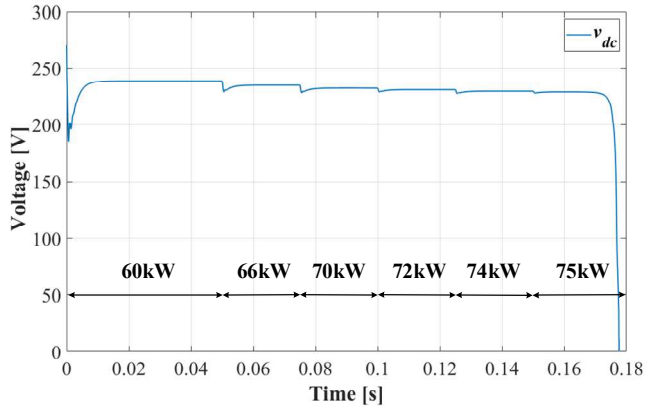

Fig. 11. Main DC bus voltage where the other two branches inject power HP converter side branch.

As it can be seen from the simulation, the DC bus voltage drops to 0 at 0.178s where 76kW is applied to the main DC bus. So 76kW load power reaches the unstable region of the system, which is acceptable compared to the calculation result.

V. CONCLUSION

In this paper, the potential power limitation is analysed for the MEA power generation concept APGC. It is found the power limitation between two three-phase-AC voltage sources and among three three-phase-AC voltage sources do exist. The detailed power limitation equations have been calculated. Corresponding verifications have been finished within MATLAB/Simulink, and the results are all following the theoretical calculation values. Further investigation will be performed to determine the best approach on optimising the APGC in terms of efficiency and bus voltage.

ACKNOWLEDGMENT

This project has received funding from the Clean Sky 2 Joint Undertaking under the European Union's Horizon 2020 research and innovation program under grant agreement No 807081.

REFERENCES

[1] T. L. Galloway, "Advanced short haul aircraft for high density markets," *Acta Astronautica,* vol. 4, no. 1–2, pp. 15-34, 1977, doi: 10.1016/0094-5765(77)90031-5.

[2] H. Hussaini, T. Yang, Y. Gao, C. Wang, G. Bai, and S. Bozhko, "Droop Coefficient Design and Optimization Using Genetic Algorithm-A Case Study of the More Electric Aircraft DC Microgrid," presented at the IECON 2022 – 48th Annual Conference of the IEEE Industrial Electronics Society, 2022.

[3] H. Hussaini *et al.*, "Accurate Line Resistance Estimation in a Multi-source Electrical Power System of the More Electric Aircraft: An Intelligent and Data-Driven Approach," presented at the 2022 IEEE Transportation Electrification Conference & Expo (ITEC), 2022.

[4] (2022). *Jet Zero Strategy Delivering net zero aviation by 2050*.

[5] Y. Zhu, Z. Wang, T. Yang, T. Dragicevic, S. Bozhko, and P. Wheeler, "Model Predictive Control for DC Offset Suppression of Dual Active Bridge Converter for More-Electric Aircraft Applications," presented at the *2021 IEEE 30th International Symposium on Industrial Electronics (ISIE)*, 2021.

[6] Y. T. Lang Xiaoyu, Hossein Balaghi Enalou, Serhiy Bozhko, Pat Wheeler, "An Enhanced Power Generation Centre for More Electric Aircraft Applications," presented at the *2018 IEEE International Conference on Electrical Systems for Aircraft, Railway, Ship Propulsion and Road Vehicles & International Transportation Electrification Conference (ESARS-ITEC)*, Nottingham, UK, 2018.

[7] G. Bai, T. Yang, S. S. Yeoh, S. Bozhko, and P. Wheeler, "An Advanced Power Generation Architecture for More-Electric Aircraft Applications," presented at the 2023 IEEE International Conference on Electrical Systems for Aircraft, Railway, Ship Propulsion and Road Vehicles & International Transportation Electrification Conference (ESARS-ITEC), 2023.

[8] R. I. Amirnaser Yazdani, *Voltage Sourced Converters in Power Systems Modeling Control and Applications*. 2010.

[9] S. S. Yeoh, M. Rashed, M. Sanders, and S. Bozhko, "Variable-Voltage Bus Concept for Aircraft Electrical Power System," *IEEE Transactions on Industrial Electronics,* vol. 66, no. 7, pp. 5634-5643, 2019, doi: 10.1109/tie.2018.2883276.

[10] S. S. Yeoh, T. Yang, L. Tarisciotti, C. I. Hill, S. Bozhko, and P. Zanchetta, "Permanent-Magnet Machine-Based Starter–Generator System With Modulated Model Predictive Control," *IEEE Transactions on Transportation Electrification,* vol. 3, no. 4, pp. 878-890, 2017, doi: 10.1109/tte.2017.273162